Green Chemistry

PAPER

View Article Online
View Journal | View Issue

Cite this: *Green Chem.*, 2021, **23**, 4466

One-pot synthesis of enzyme@metal–organic material (MOM) biocomposites for enzyme biocatalysis†

Yanxiong Pan, [a] Hui Li,[b] Mary Lenertz, [a] Yulun Han, [a] Angel Ugrinov,[a] Dmitri Kilin, [a] Bingcan Chen *[b] and Zhongyu Yang *[a]

Received 1st March 2021,
Accepted 4th May 2021

DOI: 10.1039/d1gc00775k

rsc.li/greenchem

Metal–organic frameworks/materials (MOFs/MOMs) are advanced enzyme immobilization platforms that improve biocatalysis, materials science, and protein biophysics. A unique way to immobilize enzymes is co-crystallization/co-precipitation, which removes the limitation on enzyme/substrate size. Thus far, most enzyme@MOF composites rely on the use of non-sustainable chemicals and, in certain cases, heavy metals, which not only creates concerns regarding environmental conservation but also limits their applications in nutrition and biomedicine. Here, we show that a dimeric compound derived from lignin, 5,5′-dehydrodivanillate (DDVA), co-precipitates with enzymes and low-toxicity metals, Ca^{2+} and Zn^{2+}, and forms stable enzyme@Ca/Zn–MOM composites. We demonstrated this strategy on four enzymes with different isoelectric points (IEPs), molecular weights, and substrate sizes. Furthermore, we found that all enzymes displayed slightly different but reasonable catalytic efficiencies upon immobilization in the Ca–DDVA and Zn–DDVA MOMs, as well as reasonable reusability in both composites. We then probed the structural basis of such differences using a representative enzyme and found enhanced restriction of enzymes in Zn–DDVA than in Ca–DDVA, which might have caused the activity difference. To the best of our knowledge, this is the first aqueous-phase, one-pot synthesis of a lignin-derived "green" enzyme@MOF/MOM platform that can host enzymes without any limitations on enzyme IEP, molecular weight, and substrate size. The different morphologies and crystallinities of the composites formed by Ca–DDVA and Zn–DDVA MOMs broaden their applications depending on the problem of interest. Our approach of enzyme immobilization not only improves the sustainability/reusability of almost all enzymes but also reduces/eliminates the use of non-sustainable resources. This synthesis method has a negligible environmental impact while the products are non-toxic to living things and the environment. The biocompatibility also makes it possible to carry out enzyme delivery/release for nutritional or biomedical applications *via* our "green" biocomposites.

Introduction

Metal–organic frameworks (MOFs) are advanced enzyme immobilization platforms offering enhanced enzyme protection, substrate diffusivity/selectivity, and catalytic efficiency, and thus have improved biocatalysis, energy, materials, and protein biophysics research.[1–8] Enzyme immobilization on MOFs, thus, has significantly improved the sustainability/reusability of expensive enzymes, having a positive impact on green chemistry. Thus far, many enzymes have been proved to be functional upon encapsulation into MOFs, including those smaller than MOF apertures and larger enzymes/enzyme clusters,[9–12] the latter of which often rely on the co-precipitation of enzymes with metals/ligands. The substrates, on the other hand, are often limited to those smaller than the MOF apertures. We recently found that large substrates can also be catalyzed by enzymes *via* co-precipitation, which removed the size limitation on enzymes and substrates.[13–16]

In spite of the exciting discoveries regarding co-precipitation-based enzyme immobilization, a number of concerns have been raised. For example, one way to prepare enzyme@MOFs (such as the enzyme@zeolitic-imidazolate frameworks, ZIFs) is to co-precipitate the enzyme and metal/imidazolate in the organic phase (*ca.* MeOH),[17] and the target

[a]*Department of Chemistry and Biochemistry, North Dakota State University, Fargo, ND, 58102, USA. E-mail: zhongyu.yang@ndsu.edu*
[b]*Department of Plant Sciences, North Dakota State University, Fargo, ND, 58102, USA. E-mail: Bingcan.chen@ndsu.edu*

†Electronic supplementary information (ESI) available. CCDC 2050230. For ESI and crystallographic data in CIF or other electronic format see DOI: 10.1039/d1gc00775k

enzymes have to be protected by a polymer to avoid damage by the solvent. However, this is not ideal for all enzymes. It is also possible to prepare enzyme@MOF co-precipitates in the aqueous phase (such as the biomineralization of enzymes and Zn^{2+}/imidazolate derivatives), which also produce decent crystals.[18–20] However, the ligands used in these works may chelate endogenous metal ions (such as Ca^{2+}, Cu^{2+}, and Zn^{2+}) in certain metalloproteins, thereby damaging enzyme function.[21] Lastly and most importantly, the ligands of most current MOFs are non-renewable chemicals based on petrochemical resources, some of which are not health/environment-friendly and may even possess toxicity.[22,23] This barrier raises concerns and cautions about the environmental impact of the MOFs due to the need for non-renewable petroleum resources and when applying the enzyme@MOF composites in food, nutrition, and biomedicine science/industry. Hence, alternative ligands are required.

To overcome these barriers, we are exploring alternative metals and biocompatible ligands for co-precipitation with enzymes. We found a ligand from sustainable natural sources, the lignin-derived dimeric compound 5,5′-dehydrodivanillate (DDVA), which can co-precipitate enzymes with low-toxicity metals. DDVA originates from a part of lignin,[24] a biomass from plants whose growth requires only sunlight, oxygen, and water. Furthermore, DDVA has been considered as a nutrient for certain bacteria which employ certain enzymes to convert DDVA, indicating the high biocompatibility and low toxicity of DDVA.[25,26] The metal centers, Ca^{2+} and Zn^{2+}, are also considered as less-toxic metals. Co-precipitating enzymes with Ca/Zn and DDVA resulted in layer-by-layer structures of crystal-like composites. We thus name the resultant composites Ca-/Zn-based MOMs, to distinguish them from the 3-dimensional structures of classic MOFs. The resultant enzyme@MOM composites have all the aforementioned advantages such as the ease of operation and no size limitation on enzymes and substrates. Interestingly, the enzyme@Ca–DDVA and enzyme@Zn–DDVA MOM-based composites display different morphologies and crystallinities. We tested both MOMs on four enzymes with different isoelectric points (IEP), molecular weights, and substrate sizes: lysozyme (lys, 18.7 kDa; substrate: bacterial cell walls; IEP: 9.2), lipase (53 kDa; substrate: esters; IEP: 5.8), glucose oxidase (GOx, 80 kDa; substrate: glucose; IEP 4.2), and horseradish peroxidase (HRP, 44 kDa; substrate: H_2O_2; IEP: 3–9). We found that all enzymes showed the expected catalytic activity in the enzyme@Ca–DDVA and enzyme@Zn–DDVA biocomposites, with a higher catalytic efficiency in the former. In addition, the loading capacity and reusability of the immobilized enzymes were decent. Lastly, we carried out site-directed spin labeling (SDSL)-electron paramagnetic resonance (EPR) studies[16,27–29] to probe the possible structural basis of a relatively high catalytic efficiency on a representative enzyme, and found potential origins of the activity difference.

To the best of our knowledge, this is the first report on immobilizing enzymes with arbitrary IEP, molecular weight, and substrate size in a biocompatible lignin-based "green" MOF/MOM *via* a simple, aqueous-phase, one-pot "green" synthesis. The ligand originates from lignin-derivatives which can help reduce the use of non-renewable chemicals and save petroleum sources; the compound can serve as the nutrient of certain bacteria, indicating its high biocompatibility. Also, the synthetic conditions are "green" and do not require heating, pressure, or organic solvents. These aspects open an avenue for the "green" synthesis of "sustainable" "green" enzyme@MOM composites. Different from the existing "green" MOF works,[30–38] for the first time our approach allows for the immobilization of enzymes in "green" MOMs and demonstrates the biocatalytic activity of the involved enzymes. The decent loading capacity is another advantage. The different morphologies and crystallinities of the composites formed by Ca^{2+} and Zn^{2+} make it possible to apply our composites according to the problem of interest. Our approach of enzyme immobilization not only improves the sustainability/reusability of almost all enzymes but also reduces/eliminates the use of non-sustainable resources. This synthetic method has a negligible environmental impact while the products are non-toxic to living things and the environment. The biocompatibility and/or biodegradability of metals and the DDVA ligand make it possible to carry out enzyme release for nutritional or biomedical applications *via* our "green" enzyme@MOF/MOM composites.

Results and discussion

Selection of metals and ligands

We are particularly interested in ligands derived from plants because their growth requires only sunlight, soil, and water, and because of their biocompatibility, high structural variety, and great natural sources. After a careful screening, we found that a dimeric compound derived from lignin, DDVA, can form coordination bonds with some low-toxicity metal ions such as Zn^{2+} and Ca^{2+} (as compared to other metals often encountered in MOF research) *via* their hydroxyl, carboxyl, and ether groups. Remarkably, DDVA is able to immobilize enzymes during its co-crystallization with Zn^{2+} or Ca^{2+} under a "green" condition at ambient temperature and pressure in the aqueous phase. Thus, this work is focused on the aqueous-phase co-precipitation of DDVA with Zn^{2+} or Ca^{2+} and several enzymes.

Synthesis and characterization of enzyme@Ca–DDVA and Zn–DDVA biocomposites

The reaction schemes to prepare enzyme@Ca–DDVA or Zn–DDVA in water at room temperature (RT) are shown in Fig. 1, with details being provided in the ESI.† The scanning electron microscope (SEM) images shown in Fig. 2 indicate that both composites are round shaped particles, with Ca–DDVA being larger in size than Zn–DDVA (Fig. 2a and d). The surface of Ca–DDVA shows more regular shapes while that of Zn–DDVA possesses flower-like porous materials (Fig. 2b *versus* 2e). The incorporation of enzymes in both composites was confirmed *via* attenuated total reflectance (ATR)–Fourier transformation infrared (FTIR) spectroscopy (Fig. S1†), wherein the appear-

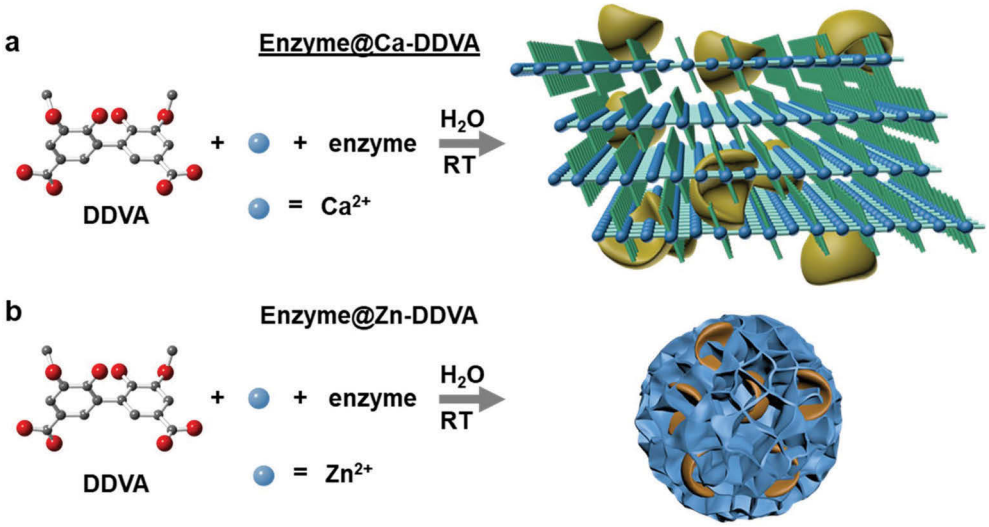

Fig. 1 Reaction schemes of the preparation of enzyme@Ca–MOM composites. (a) Preparation of enzyme@Ca–DDVA in water at room temperature (RT). (b) Preparation of enzyme@Zn–DDVA in water at RT. The morphologies of the resultant composites are derived based on our experimental findings (see Fig. 2). Yellow/orange models represent the enzymes in the composites.

ance of the 1640 cm^{-1} peak upon enzyme incorporation due to the protein C=O stretching vibration indicates the presence of protein molecules. We also used fluorescein isothiocyanate (FITC) to label each enzyme and incorporated the labeled enzymes into Ca–DDVA and Zn–DDVA. The resultant confocal fluorescent images confirmed the successful inclusion of enzymes (representative data on lys are shown in Fig. 2c and f).

The powder X-ray diffraction (PXRD) patterns of enzyme@Ca–DDVA are similar to the single-crystal XRD pattern of pure Ca–DDVA prepared at a higher temperature (60 °C; Fig. 3a), which indicates a layer-by-layer structure. Within each layer, as shown in Fig. 4a, "sub-layers" are also present. A closer look at the crystal structure indicates two categories of Ca^{2+} coordination. First, as shown in Fig. 4b, each Ca^{2+} ion is coordinated with an ether and a hydroxyl group from a DDVA above and those from another DDVA below; four water molecules are also coordinated. This category of Ca^{2+} coordination seems to be the driving force connecting the sub-layers. Second, within a sub-layer, two Ca^{2+} in close proximity are stabilized by four DDVAs. Each Ca^{2+} is coordinated with an ether and a hydroxyl group from a DDVA (see OH_1 and $ether_1$ for the top Ca^{2+} of Fig. 4c and OH_4 and $ether_4$ for the bottom Ca^{2+}) and a carboxyl group from another DDVA (see $COOH_2$ for the top Ca^{2+} of Fig. 4c and $COOH_3$ for the bottom Ca^{2+}). The carboxyl groups keep two Ca^{2+} ions in close proximity. Interestingly, in each DDVA, there is one carboxyl group that does not participate in coordination, which may facilitate enzyme contact and thus, incorporation. The diffraction pattern of Zn–DDVA suggests that only an amorphous structure was formed (Fig. 3b), consistent with the irregular, porous materials shown by SEM (Fig. 2e). The co-crystallization of metals and ligands depends on not only the orbital/charge/size of the metal but also the structure of the ligand, both of which determine how the metal coordinates with the ligand. To form crystals, Zn^{2+} is more preferential to coordinate with imidazolates while Ca^{2+} is commonly seen to coordinate with carboxylates (such as terephthalic acid, also known as BDC).[19,39] We observed a relatively rare case that Zn^{2+} coordinates with a carboxylate compound, DDVA, likely caused by the presence and specific arrangement of the multiple carboxylate groups in DDVA (since Zn^{2+} and BDC do not form crystals at room temperature under aqueous conditions). Currently, we do not have definitive evidence to conclusively identify the origins of low crystallinity of Zn–DDVA in comparison with Ca–DDVA. We do not have a clear picture of the crystal structure of Zn–DDVA either. Our judgement of the partial crystalline nature of Zn–DDVA was solely based on the broadened PXRD pattern. Revealing such a mystery is our on-going work.

The thermal gravimetric analysis (TGA) data of Ca–/Zn–DDVA MOMs in the absence and presence of enzymes indicate the entrapment of enzymes in both composites (for the representative data see Fig. 3c and d). The presence of enzyme does not seem to significantly impact the thermostability of Ca–DDVA and Zn–DDVA alone. The amounts of entrapped enzymes in both composites were determined using a bicinchoninic acid (BCA) assay.[40] Typically, the enzyme loading capacities of ~10% and ~6.7% (w/w) were found for enzyme@Ca–DDVA and enzyme@Zn–DDVA, respectively, comparable to or slightly higher than those reported in the literature.[10] Only the representative data of XRD and TGA using lys@Ca–DDVA or Zn–DDVA are shown here. Other enzymes display similar trends/patterns and are not shown for conciseness of the paper.

Catalytic activity of enzymes on both composites

To generalize our platform for enzyme incorporation, we used four enzymes that are commonly studied as models in biocata-

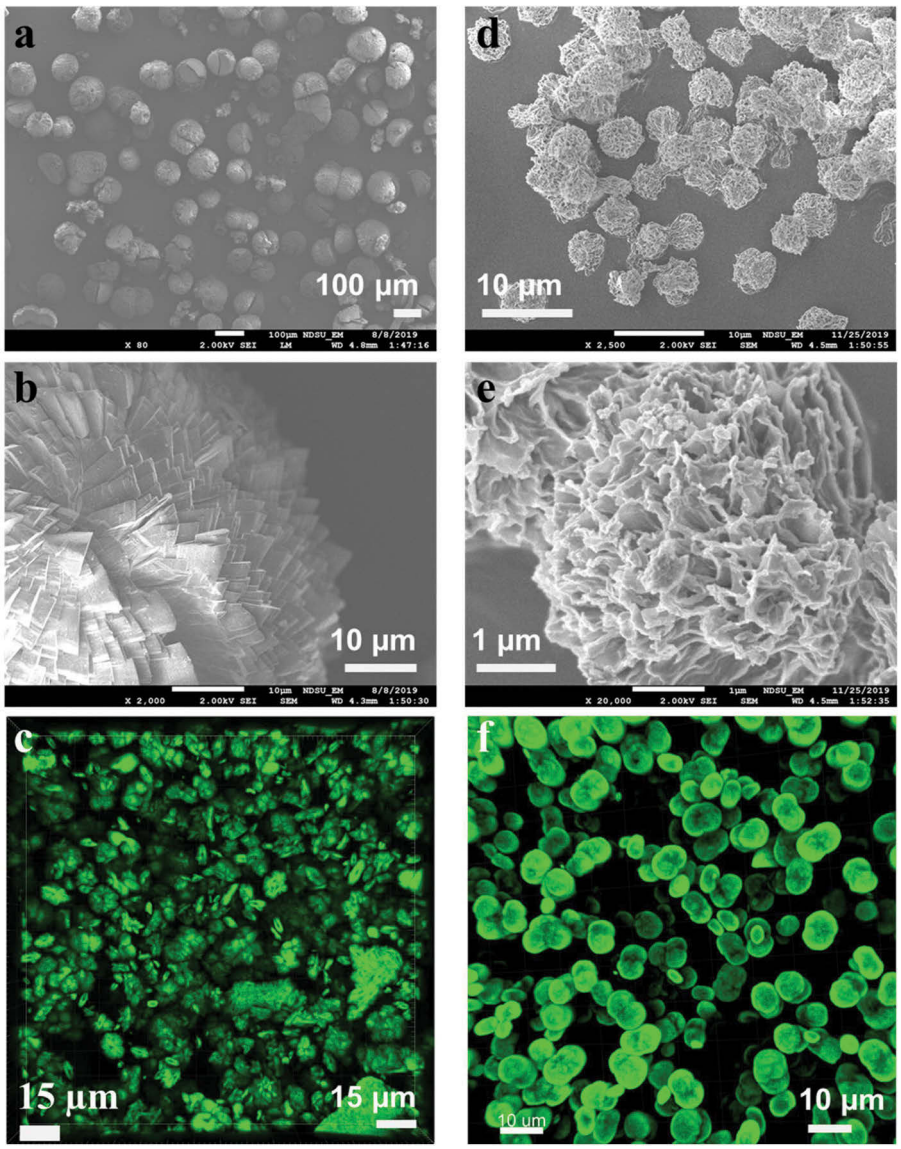

Fig. 2 Images of the enzyme@MOM composites. (a and b) The SEM images of lys@Ca–DDVA at different length scales. (c) The confocal fluorescence images of FITC-labeled lys in Ca–DDVA. (d and e) The SEM images of lys@Zn–DDVA at different length scales. (f) The confocal fluorescence images of FITC-labeled lys Zn–DDVA. (c) and (f) Indicate the successful inclusion of the representative enzyme in each composite.

lysis: lys, lipase, GOx, and HRP. Each enzyme was hosted in Ca–DDVA and Zn–DDVA, respectively (for characterization see above). The catalytic activity of each enzyme in each MOM-based composite was then investigated using the corresponding activity assays.

The physiological substrate of lys is the bacterial cell walls.[41] To quantify lys activity, the commercial activity kit EnzChek® Lysozyme Assay Kit (see the ESI†) was employed, which monitors the generation of a fluorescence signal using the fluorescein labeled Micrococcus lysodeikticus cell wall as the substrate. As controls, the product generation as a function of free lys concentration is close to linear (Fig. S5†), while the DDVA alone, Ca–DDVA (no lys), and Zn–DDVA (no lys) did not generate any product (Fig. S6†). The catalytic activities of free lys, lys@Ca–DDVA, and lys@Zn–DDVA for the same enzyme loading amount (as determined by the BCA assay) are shown in Fig. 5a and b. Both composites showed a reduced catalytic efficiency against the same substrate as compared to the free lys, the reason being the reduced mobility of composites and the partial exposure of the lys enzyme on the composite surface (for structural basis see below). Lys@Zn–DDVA displays a lower catalytic efficiency than lys@Ca–DDVA, likely because of the rugged surface of the Zn–DDVA composite as compared to the smooth and large surface of Ca–DDVA (see SEM images of Fig. 2), which may prevent effective contact with the large substrate. The enzymatic kinetic parameters, V_{max} and K_m, were calculated under increasing substrate concentrations and are summarized in Table 1, which confirmed the relative cata-

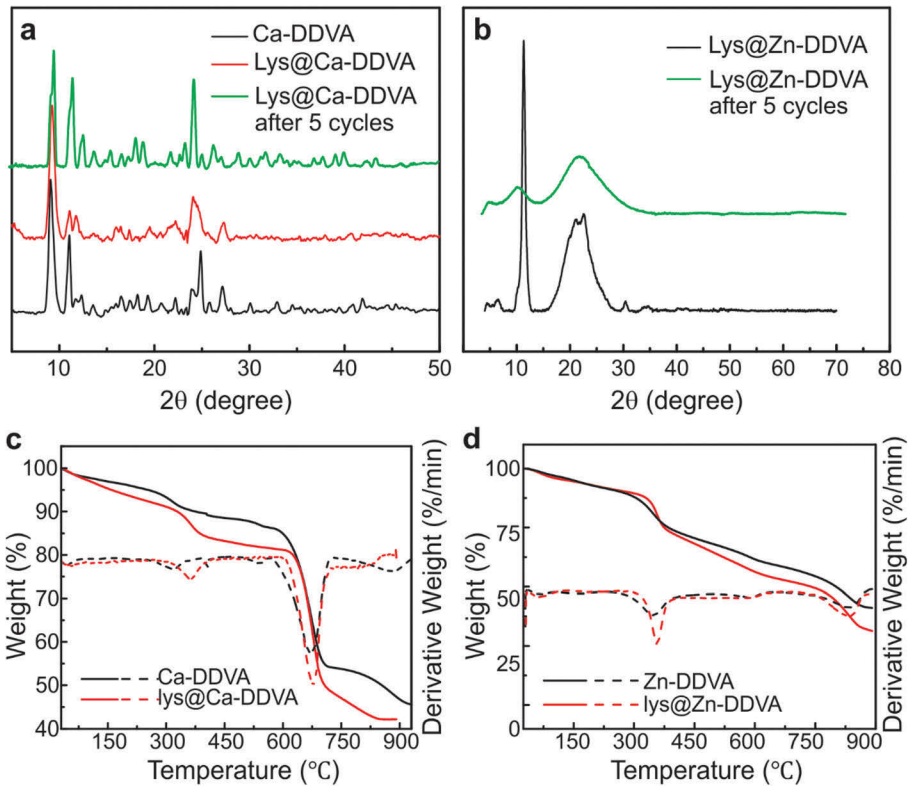

Fig. 3 Characterization of the enzyme@Ca–/Zn–MOM composites. (a) The XRD data of the lys@Ca–DDVA composites developed in this work before and after 5 catalytic cycles (green). (b) The PXRD data of lys@Zn–DDVA before and after 5 catalytic cycles (green). (c) The TGA data of lys@Ca–DDVA as representatives of enzyme@MOM platforms suggested the inclusion of the enzyme in the composites. (d) The TGA data of lys@Zn–DDVA.

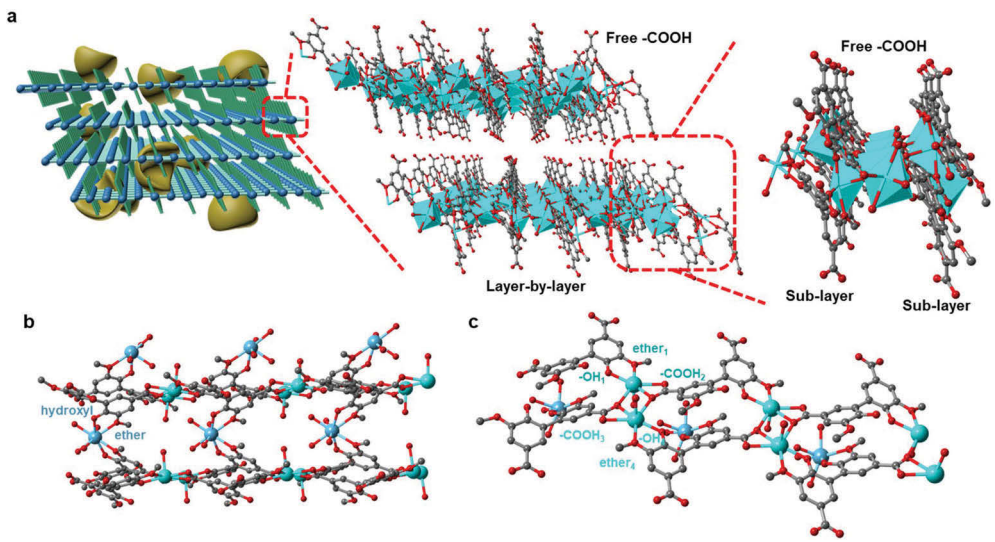

Fig. 4 Structure of Ca–DDVA. (a) The structure of the single-crystal Ca–DDVA at different length scales. (b) The first Ca^{2+} coordination: each Ca^{2+} in between the sub-layers is coordinated with an ether and a hydroxyl group. (c) The second Ca^{2+} coordination: two Ca^{2+} ions in close proximity. Each Ca^{2+} in the same sub-layer is coordinated with an ether and a hydroxyl group from one DDVA (see subscripts 1 and 4) and a carboxyl group from an adjacent DDVA (see subscripts 2 and 3). The carboxyl groups keep two Ca^{2+} ions in close proximity. In each DDVA, there is one carboxyl group that does not participate in coordination.

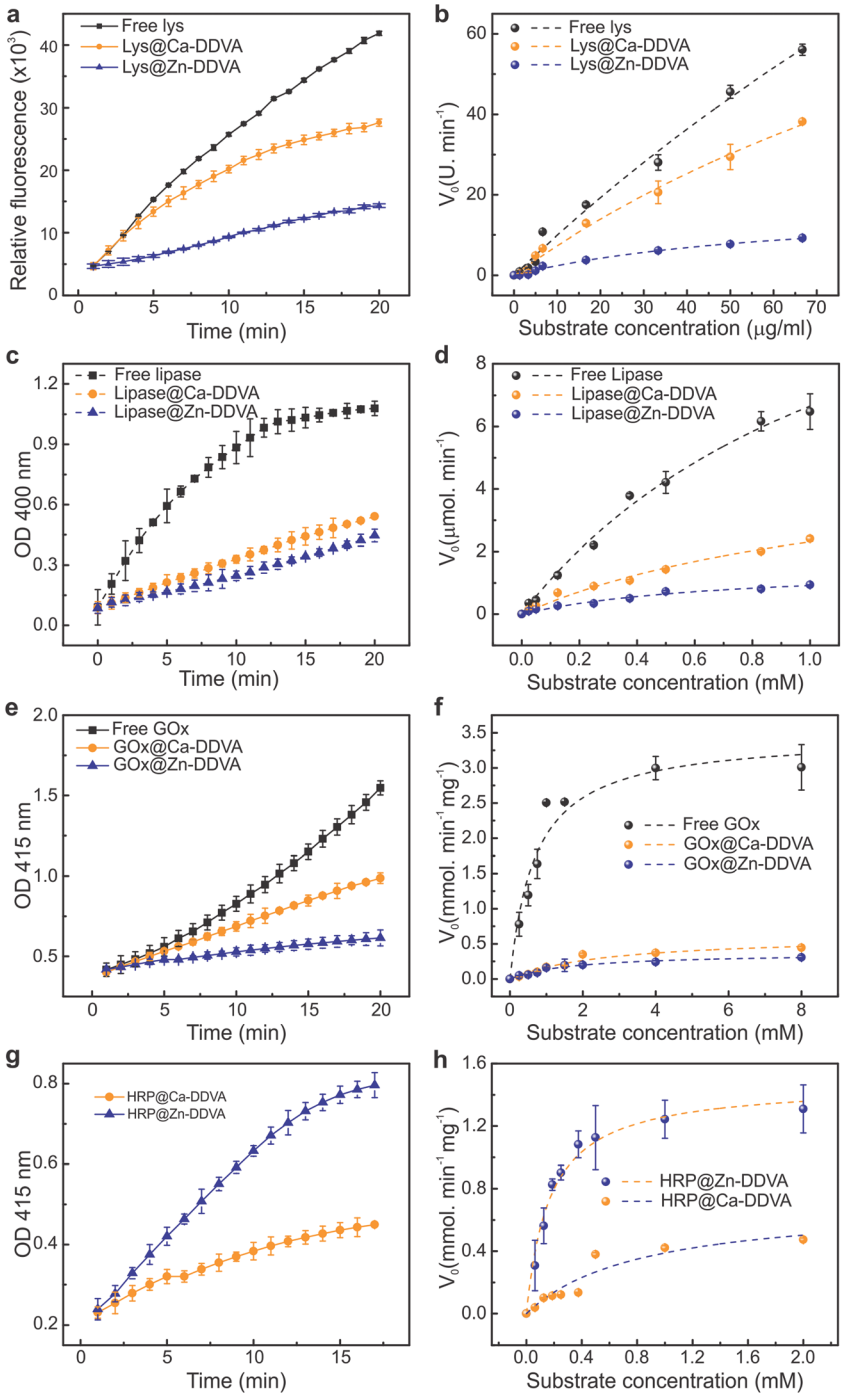

Fig. 5 Activity assays of each enzyme@MOM composites. (a, c, e and g) Representative data of the catalytic activity assays of lys (a), lipase (c), GOx (e), and HRP (g) upon loading into each composite. (b, d, f and h) The enzymatic kinetics analysis with fitting of each enzyme. For data analysis and fitting, see the main text and the ESI.†

Table 1 The kinetic parameters of the hydrolysis of Micrococcus lysodeikticus cell wall catalysed by free lys and the lys@Ca–DDVA/Zn–DDVA composites obtained *via* the Michaelis–Menten method

Parameters	V_{max} (U min^{-1})	K_m (U)	R^2
Lys	316.4 ± 194.5	308.3 ± 222.0	0.9889
Lys@Ca–DDVA	136.3 ± 44.1	175.8 ± 73.4	0.9910
Lys@Zn–DDVA	18.1 ± 2.8	64.8 ± 16.9	0.9883

lytic efficiency discussed above. Error bars were obtained *via* three repeated measurements under the same conditions (substrate concentration, buffer pH, *etc.*).

The lipase catalytic activity was assessed by quantifying the generation of acetic acid and 4-nitrophenol when 4-nitrophenyl acetate is hydrolyzed by lipase. Here the 4-nitrophenol has a UV-vis absorption at 400 nm which was monitored over

time.[42] Upon confirming DDVA alone, Ca–DDVA (no lipase), and Zn–DDVA (no lipase) did not generate any 4-nitrophenol (Fig. S7†), for the same enzyme loading amount, free lipase, lipase@Ca–DDVA, and lipase@Zn–DDVA composites showed the formation of 4-nitrophenol (Fig. 5c). Free lipase showed a much higher catalytic efficiency than the composites, likely due to the reduced substrate diffusion within our MOM network. Lipase@Ca–DDVA showed a slightly higher efficiency than lipase@Zn–DDVA. The calculated V_{max} and K_m values (Fig. 5d, right and Table 2) also indicate the same trend.

HRP is needed for GOx activity assessment as described in the literature.[9,43] In detail, GOx degrades glucose and generates glucono–lactone and H_2O_2; HRP was then added together with the produced H_2O_2 to convert the 2,2′-azino-bis(3-ethylbenzothiazoline-6-sulfonic acid) diammonium salt (ABTS) to $ABTS^{\bullet+}$. The latter displays a UV-vis absorption at 415 nm, which was monitored over time.[44,45] With HRP, upon confirming DDVA, Ca–DDVA (no lipase), and Zn–DDVA (no lipase) did not generate $ABTS^{\bullet+}$ for the same GOx amount, free GOx and the two composites showed the formation of $ABTS^{\bullet+}$ (Fig. 5e), although the composites showed a much lower efficiency than free GOx, likely due to the reduced enzyme mobility and substrate diffusivity. GOx@Ca–DDVA stills shows a slightly higher efficiency than GOx@Zn–DDVA. The calculated V_{max} and K_m values (Fig. 5f and Table 3) also indicate the same trend.

HRP activity was studied similarly except that H_2O_2 was provided to free HRP and the HRP@Ca–DDVA and HRP@Zn–DDVA composites (Fig. 5g). Different from the above trends, HRP@Zn–DDVA showed a slightly higher efficiency than HRP@Ca–DDVA (Fig. 5h and Table 3). Lastly, both Ca–DDVA and Zn–DDVA are able to encapsulate both GOx and HRP and carry out cascade biocatalysis. The representative data set is shown in the ESI (Fig. S8†).

Reusability and stability of the composites

The reusability of Ca–DDVA and Zn–DDVA was assessed using lipase as the representative enzyme. We chose lipase because of the convenience of testing lipase activity, which requires less time and materials/resources. The V_{max} value after 5 reuse cycles was calculated as described above and plotted as the relative activity in % as shown in Fig. 6. Both composites showed more than 80% reusability for lipase, with lipase@Zn–DDVA showing a higher relative activity than lipase@Ca–DDVA. The composites are stable after these five repeated cycles as indicated by the PXRD data before and after 5 reuse cycles (Fig. 3a and b, green). The amorphous Zn–DDVA seemed to lose some more crystallinity as indicated by the broadened peaks. However, the particles were present the whole time, enabling their high reusability. The drop in the relative activity (Fig. 6) is likely caused by a combination of enzyme function loss (due to multiple cycles) and the enzyme quantity loss (due to sample loss). To quantify the enzyme loss between washes, we prepared a series of identical aliquot samples and performed the reusability test in parallel. After each cycle, we disassembled one aliquot and measured the entrapped enzyme. We found that the enzyme loss was small (less ~1% loss), which can be considered negligible when evaluating their reusability and V_{max} values.

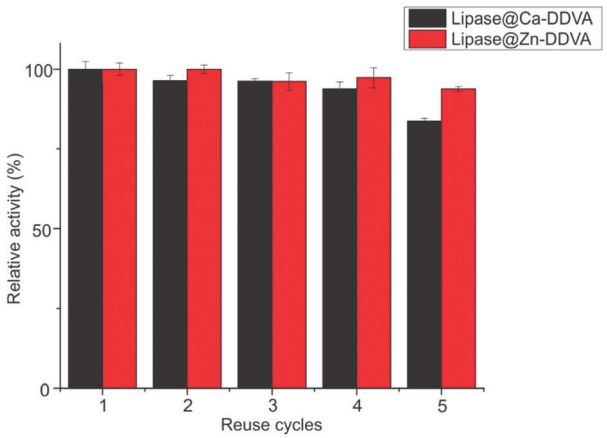

Fig. 6 The relative reusability of the Ca–/Zn–DDVA MOF composites when lipase is studied as the model enzyme. Within 5 cycles, both composites showed ~>80% relative catalytic efficiency. Lipase@Zn–DDVA showed a higher reusability than lipase@Ca–DDVA.

Enzyme immobilization using MOMs based on Ca–DDVA and Zn–DDVA improved the stability of the enzyme. In particular, as shown in Fig. S10,† the relative activity of lipase after storage on bench for 7 days is comparable to that of lipase@Ca–DDVA. Interestingly, lipase@Zn–DDVA seemed to show a better stability than Ca–DDVA and free enzyme, in line with the better reusability of lipase@Zn–DDVA. In pure water at 4 °C, the composites are stable for at least 2 weeks. Weakly basic pHs are required when using our composites for biocatalytic reactions. In fact, most enzymes (especially the four representatives discussed in this work) can have reasonable catalytic performance, indicating that our platform can be applicable to many enzymes. We are continuously discovering other green ligands to form acid-stable composites that can immobilize enzymes.

Table 2 The kinetic parameters of free lipase and the synthesized lipase@Ca–DDVA/Zn–DDVA composites

Parameters	V_{max} (μmol min^{-1})	K_m (μM)	R^2
Lipase	37.0 ± 4.7	0.97 ± 0.21	0.989
Lipase@Ca–DDVA	9.7 ± 1.3	0.94 ± 0.21	0.988
Lipase@Zn–DDVA	5.2 ± 0.4	0.56 ± 0.94	0.989

Table 3 The kinetic parameters of the GOx@Ca–DDVA/Zn–DDVA and HRP@Ca–DDVA/Zn–DDVA composites

Parameters	V_{max} (mmol min^{-1} mg^{-1})	K_m (mM)	R^2
GOx@Ca–DDVA	0.62 ± 0.09	2.69 ± 0.81	0.939
GOx@Zn–DDVA	0.37 ± 0.03	1.76 ± 0.35	0.964
HRP@Ca–DDVA	0.71 ± 0.15	0.83 ± 0.36	0.972
HRP@Zn–DDVA	1.47 ± 0.08	0.17 ± 0.2	0.969

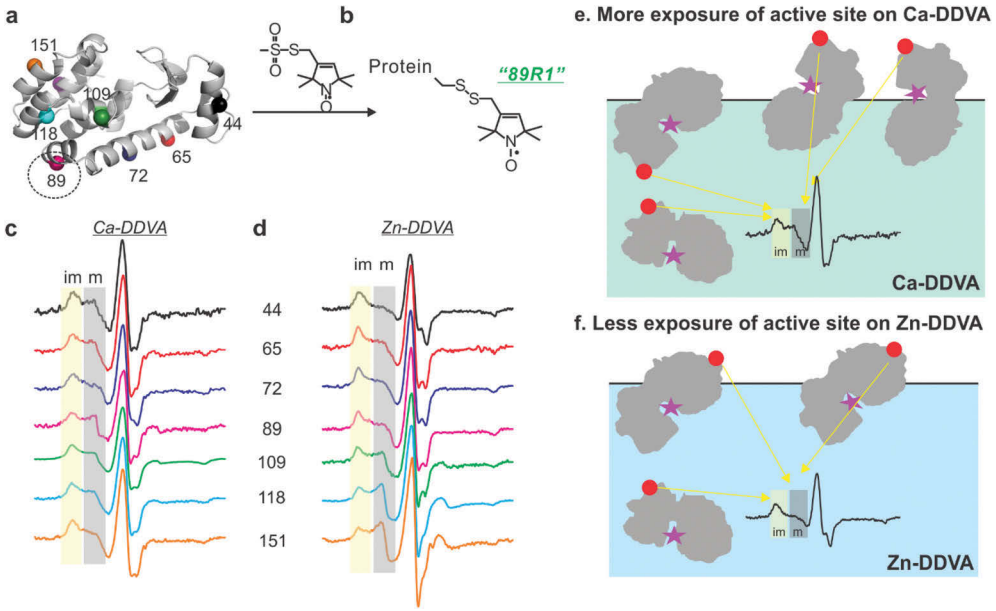

Fig. 7 Probing the structural basis of the catalytic behavior using lys@MOM as the model system. (a) The surface residues that are spin labeled with a nitroxide (b) for structural study. (c and d) The EPR spectrum of each labeled mutant upon encapsulation into each DDVA-based composite. (e, f) Schematic illustration of the exposable region of lys on the Ca–DDVA and Zn–DDVA surface as determined by EPR. Star = lys active site.

Structural basis of large substrate biocatalysis

Similar to our recent finding,[16] we propose that the partial exposure of lys encapsulated in the MOM-based composite is the cause of enzyme contact with a large-size substrate. Here we employ the similar principles developed in our recent work[16] to determine the chance of exposing different lys regions above the surface of each of the DDVA-based MOMs developed in this work. In brief, we site-specifically labeled (Fig. 7a and b) a model enzyme, lys, and determined the backbone dynamics of multiple labeled sites on lys using Electron Paramagnetic Resonance (EPR) spectroscopy (Fig. 7c and d). This approach is immune of the complexities caused by the MOF/MOM backgrounds and is sensitive to ns-scale protein sidechain motion.[18] In addition, a labeled protein residue exposed above the MOF/MOM crystal to the reaction medium would display enhanced dynamics (often designated as the "m" component which stands for mobile) as compared to those buried inside of the MOF/MOM ("im" component stands for immobile; see Fig. 7c–f). The relative population of each case can be determined *via* spectral simulation if both cases exist for the same labeled residue (Fig. 7e and f).[16,46–48]

In detail, as shown in Fig. 7c and d, although both "m" and "im" components are observed for each mutant, there is a significant increase in the "m" component (due to exposure above the crystal surface) in Ca–DDVA in the N-terminus and near the active site (see the high "m" peak intensity for residues 44 and 65) as compared to the "m" component intensity in Zn–DDVA in the same region. In contrast, in Zn–DDVA, the C-terminus of lys shows enhanced chance of exposure (see the high "m" peak intensity for residues 109, 118, and 151). Because the C-terminus is further away from the active site, our structural study indicates that there is a high chance for lys to display lower catalytic efficiency in Zn–DDVA due to the less chance of active site exposure to the reaction medium (and contact the large substrate; Fig. 7f). Spectral simulations detailed in the ESI† also confirmed the same conclusion, wherein the N-terminal residues of lys in Ca–DDVA show higher "m" component populations (47.5% and 58.5% for residues 44 and 65) than those in Zn–DDVA (28.0% and 49.2% for residues 44 and 65), indicating that the N-terminus has a higher chance of being exposed in the former. Interestingly, for the "im" component which was caused by the enzyme buried under the MOM surface, the ordering parameters (see C_{20} and C_{22} in Tables S3 and S4†) indicate a higher degree of restriction in the sidechain motion of the labeled sites in Zn–DDVA than that in Ca–DDVA. Also, the rate parameters (see $R_{z,im}$ in Tables S3 and S4†) suggest a reduced sidechain motion of the labeled sites in Zn–DDVA as compared to that in Ca–DDVA. These together lead to a speculation that most enzymes (3 out of 4, in our study) may encounter more restriction in Zn–DDVA, which results in the reduced catalytic efficiency.

Discussions

The different properties of the Ca– and Zn–DDVA composites make it possible to apply our composites depending on the problem of interest. For example, if the target system can tolerate one metal over the other, then one can choose the composite based on such a need. In addition, although the catalytic efficiency of enzyme@Ca–DDVA seems to be better than that of

enzyme@Zn–DDVA in 3 out of the 4 studied enzymes, a unique advantage of the enzyme@Zn–DDVA composites is that they can diffuse into smaller gaps and/or make more efficient contact with large, rigid substrates (such as those frequently encountered in food research). It is also promising to use the enzyme@Zn–DDVA composites for penetrating certain biological barriers in biomedical applications. Lastly, lipase@Zn–DDVA displayed a higher reusability than lipase@Ca–DDVA, indicating the possibility that enzyme@Zn–DDVA can be reused for more catalytic cycles. Thus, the enzyme@Zn–DDVA composites are also useful and worth developing/investigating.

Although only a minor drawback was proved by various experiments *via* different approaches, the cytotoxicity of MOF materials always raises concerns in nutritional and/or medical applications.[49–53] The high biocompatibility and biodegradability of the DDVA ligand and the low toxicity of Ca^{2+} and Zn^{2+} metal ions will likely overcome, or, at least, reduce these concerns. Furthermore, under certain conditions, the loaded enzymes in our platforms may be released by disassembling the MOF/MOM scaffolds, making it possible to deliver the enzyme to the desired locations. This effort will broaden the application of our composites in food, nutrition, and health.

Due to the complex coordination manner between Ca^{2+} and DDVA, it is highly possible that such stringent coordination conditions (stoichiometry and relative arrangement of ions and ligand molecules in the 3D space) cannot be met in metalloproteins. This indicates that our platform may be used to encapsulate metalloproteins containing Ca^{2+}, Cu^{2+}, or Zn^{2+}, further generalizing our method to more enzymes.

The differences in the catalytic efficiencies of the studied enzymes on Ca–DDVA and Zn–DDVA are not so clear at this moment. We suspect that the catalytic efficiency depends on many complex factors such as the substrate diffusion efficiency, the collision efficiency between the enzyme and the substrate, and even the dynamics of the encapsulated enzymes in each MOF. These factors can further depend on the surface properties, size, and even the shape of the composites. For lys, a large-substrate enzyme, we utilized the SDSL-EPR approach to probe the possible explanation. However, more work is needed to understand the structural basis of the performance of the other three enzymes, which is our on-going research direction.

Experimental

Materials and measurements

All chemicals and biochemical supplies were purchased from commercially available resources in high purity; the involved experiments were carried out without purification. All characterization methods, including powder X-ray diffraction (PXRD), single-crystal X-ray diffraction (XRD), scanning electron microscopy (SEM), thermal gravimetric analysis (TGA), and FTIR spectroscopy, were applied to the involved materials following the previously published procedures and using equipment described in our recent work.[29] Expression, purification, and spin labeling of the involved lysozyme mutants were performed following the procedures described in our recent work.[16] For EPR measurements, each protein mutant was transferred into a borosilicate capillary tube (0.70 mm i.d./1.00 mm o.d.; Wilmad Labglass, Inc.) immediately after mixing the channel-materials. Data were acquired using a Varian E-109 spectrometer equipped with a cavity resonator. All continuous wave (CW) EPR spectra were obtained with a power of 200 mW, a modulation frequency of 100 kHz, and a modulation amplitude of 1.0 G.

Conclusions

We discovered that the biocompatible ligand DDVA from sustainable natural sources can co-precipitate with enzyme and Ca^{2+} or Zn^{2+} in the aqueous phase at room temperature. This ligand can be derived from the renewable biomass, lignin, whose growth only requires sunlight, oxygen, and water while the low toxicity of Ca^{2+} and Zn^{2+} make the resultant MOM a "green" enzyme@MOM composite. We demonstrated this platform on four enzymes with different IEPs, molecular weights, and substrate sizes, all of which showed the expected catalytic performance. Both composites displayed decent enzyme loading capacities and reusability. To the best of our knowledge, this is the first one-pot "green" synthesis of biocompatible "green" enzyme@MOM composites that can be derived from sustainable resources and generalized to encapsulate most enzymes with no limitation on IEP, molecular weight, and/or substrate size. The different morphologies and crystallinities of the composites formed by Ca^{2+} and Zn^{2+} make it possible to apply our composites depending on the problem of interest. Our approach improves the sustainability/reusability of almost all enzymes as well as reduces/eliminates the use of non-sustainable resources while having a negligible environmental impact. The products are non-toxic to living things and the environment. The biocompatibility and/or biodegradability of metals and the DDVA ligand make it possible to carry out enzyme release for nutritional or biomedical applications *via* our enzyme@MOF composites.

Author contribution

B. C., and Z. Y. conceived and designed the research. Y. P., H. L., and M. L. performed the synthesis and catalytic assays. Y. P. and H. L. acquired the EPR data and carried out the data analysis. Y. H., A. U. and D. K. assisted in all data analysis and interpretation. All authors participated in drafting the manuscript and approved the final version.

Conflicts of interest

The authors claim no conflict of interest.

Acknowledgements

This work is supported by the NSF (#1942596 to Z. Y.) and NDSU New Faculty Startup Funds and the USDA-NIFA Grant 2021-67021-34002 (to B. C.). We appreciate Prof. Hubbell for generously providing the EPR spectral simulation package.

Notes and references

1 X. Lian, Y. Fang, E. Joseph, Q. Wang, J. Li, S. Banerjee, C. Lollar, X. Wang and H.-C. Zhou, *Chem. Soc. Rev.*, 2017, **46**, 3386–3401.
2 A. Kirchon, L. Feng, H. F. Drake, E. A. Joseph and H.-C. Zhou, *Chem. Soc. Rev.*, 2018, **47**, 8611–8638.
3 X. Wang, P. C. Lan and S. Ma, *ACS Cent. Sci.*, 2020, **6**, 1497–1506.
4 M. B. Majewski, A. J. Howarth, P. Li, M. R. Wasielewski, J. T. Hupp and O. K. Farha, *CrystEngComm*, 2017, **19**, 4082–4091.
5 P. Li, Q. Chen, T. C. Wang, N. A. Vermeulen, B. L. Mehdi, A. Dohnalkova, N. D. Browning, D. Shen, R. Anderson, D. A. Gómez-Gualdrón, F. M. Cetin, J. Jagiello, A. M. Asiri, J. F. Stoddart and O. K. Farha, *Chem*, 2018, **4**, 1022–1034.
6 R. J. Drout, L. Robison and O. K. Farha, *Coord. Chem. Rev.*, 2019, **381**, 151–160.
7 E. Gkaniatsou, C. M. Sicard, R. M. Ricoux, J.-P. Mahy, N. Steunou and C. Serre, *Mater. Horiz.*, 2017, **4**, 55–63.
8 A. J. Howarth, Y. Liu, P. Li, Z. Li, T. C. Wang, J. T. Hupp and O. K. Farha, *Nat. Rev. Mater.*, 2016, **1**, 15018.
9 W.-H. Chen, M. Vázquez-González, A. Zoabi, R. Abu-Reziq and I. Willner, *Nat. Catal.*, 2018, **1**, 689–695.
10 F. K. Shieh, S. C. Wang, C. I. Yen, C. C. Wu, S. Dutta, L. Y. Chou, J. V. Morabito, P. Hu, M. H. Hsu, K. C. W. Wu and C. K. Tsung, *J. Am. Chem. Soc.*, 2015, **137**, 4276–4279.
11 G. Chen, X. Kou, S. Huang, L. Tong, Y. Shen, W. Zhu, F. Zhu and G. Ouyang, *Angew. Chem., Int. Ed.*, 2020, **59**, 2867–2874.
12 Y. Li, P. Zhao, T. Gong, H. Wang, X. Jiang, H. Cheng, Y. Liu, Y. Wu and W. Bu, *Angew. Chem., Int. Ed.*, 2020, **132**, 22726–22732.
13 J. Farmakes, I. Schuster, A. Overby, L. Alhalhooly, M. Lenertz, Q. Li, A. Ugrinov, Y. Choi, Y. Pan and Z. Yang, *ACS Appl. Mater. Interfaces*, 2020, **12**, 23119–23126.
14 S. Neupane, K. Patnode, H. Li, K. Baryeh, G. Liu, J. Hu, B. Chen, Y. Pan and Z. Yang, *ACS Appl. Mater. Interfaces*, 2019, **11**, 12133–12141.
15 Q. Li, Y. Pan, H. Li, L. Alhalhooly, Y. Li, B. Chen, Y. Choi and Z. Yang, *ACS Appl. Mater. Interfaces*, 2020, **12**, 41794–41801.
16 Y. Pan, H. Li, J. Farmakes, F. Xiao, B. Chen, S. Ma and Z. Yang, *J. Am. Chem. Soc.*, 2018, **140**, 16032–16036.
17 F. Lyu, Y. Zhang, R. N. Zare, J. Ge and Z. Liu, *Nano Lett.*, 2014, **14**, 5761–5765.
18 H. An, J. Song, T. Wang, N. Xiao, Z. Zhang, P. Cheng, H. Huang, S. Ma and Y. Chen, *Angew. Chem.*, 2020, **59**, 16764–16769.
19 Y. Pan, Q. Li, H. Li, J. Farmakes, A. Ugrinov, X. Zhu, Z. Lai, B. Chen and Z. Yang, *Chem. Catal.*, 2021, DOI: 10.1016/j.checat.2021.03.001.
20 K. Liang, R. Ricco, C. M. Doherty, M. J. Styles, S. Bell, N. Kirby, S. Mudie, D. Haylock, A. J. Hill, C. J. Doonan and P. Falcaro, *Nat. Commun.*, 2015, **6**, 7240.
21 R. H. Holm, P. Kennepohl and E. I. Solomon, *Chem. Rev.*, 1996, **96**, 2239–2314.
22 R. S. Forgan, *Encycl. Inorg. Bioinorg. Chem.*, 2014, 1–13, DOI: 10.1002/9781119951438.eibc2192.
23 I. Imaz, M. Rubio-Martínez, J. An, I. Solé-Font, N. Rosi and D. Maspoch, *Chem. Commun.*, 2011, **47**, 7287–7302.
24 N. Kamimura, S. Sakamoto, N. Mitsuda, E. Masai and S. Kajita, *Curr. Opin. Biotechnol.*, 2019, **56**, 179–186.
25 X. Peng, E. Masai, Y. Katayama and M. Fukuda, *Appl. Environ. Microbiol.*, 1999, **65**, 2789.
26 T. Sonoki, T. Obi, S. Kubota, M. Higashi, E. Masai and Y. Katayama, *Appl. Environ. Microbiol.*, 2000, **66**, 2125.
27 W. L. Hubbell, C. J. López, C. Altenbach and Z. Yang, *Curr. Opin. Struct. Biol.*, 2013, **23**, 725–733.
28 C. Altenbach, C. J. López, K. Hideg, W. L. Hubbell, Z. Q. Peter and W. Kurt, in *Methods in Enzymology*, Academic Press, 2015, vol. 564, pp. 59–100.
29 Q. Sun, Y. Pan, X. Wang, H. Li, J. Farmakes, B. Aguila, Z. Yang and S. Ma, *Chem*, 2019, **5**, 3184–3195.
30 S. Kumar, S. Jain, M. Nehra, N. Dilbaghi, G. Marrazza and K.-H. Kim, *Coord. Chem. Rev.*, 2020, **420**, 213407.
31 S. Bao, J. Li, B. Guan, M. Jia, O. Terasaki and J. Yu, *Matter*, 2020, **3**, 498–508.
32 L. Xu, C.-Y. Xing, D. Ke, L. Chen, Z.-J. Qiu, S.-L. Zeng, B.-J. Li and S. Zhang, *ACS Appl. Mater. Interfaces*, 2020, **12**, 3032–3041.
33 J. J. Gassensmith, H. Furukawa, R. A. Smaldone, R. S. Forgan, Y. Y. Botros, O. M. Yaghi and J. F. Stoddart, *J. Am. Chem. Soc.*, 2011, **133**, 15312–15315.
34 J. Yang, C. A. Trickett, S. B. Alahmadi, A. S. Alshammari and O. M. Yaghi, *J. Am. Chem. Soc.*, 2017, **139**, 8118–8121.
35 D. Wu, J. J. Gassensmith, D. Gouvêa, S. Ushakov, J. F. Stoddart and A. Navrotsky, *J. Am. Chem. Soc.*, 2013, **135**, 6790–6793.
36 K. J. Hartlieb, J. M. Holcroft, P. Z. Moghadam, N. A. Vermeulen, M. M. Algaradah, M. S. Nassar, Y. Y. Botros, R. Q. Snurr and J. F. Stoddart, *J. Am. Chem. Soc.*, 2016, **138**, 2292–2301.
37 H. Reinsch, *Eur. J. Inorg. Chem.*, 2016, **2016**, 4290–4299.
38 Y. Feng, Y. Bi, W. Zhao and T. Zhang, *J. Mater. Chem. A*, 2016, **4**, 7596–7600.
39 K. Sumida, M. Hu, S. Furukawa and S. Kitagawa, *Inorg. Chem.*, 2016, **55**, 3700–3705.
40 P. K. Smith, R. I. Krohn, G. T. Hermanson, A. K. Mallia, F. H. Gartner, M. D. Provenzano, E. K. Fujimoto, N. M. Goeke, B. J. Olson and D. C. Klenk, *Anal. Biochem.*, 1985, **150**, 76–85.
41 D. J. Vocadlo, G. J. Davies, R. Laine and S. G. Withers, *Nature*, 2001, **412**, 835–838.
42 K. Nie, Q. An and Y. Zhang, *Nanoscale*, 2016, **8**, 8791–8797.

43 Y. Zhang, S. Tsitkov and H. Hess, *Nat. Commun.*, 2016, **7**, 13982.
44 Y. Zhang and H. Hess, *Anal. Chem.*, 2020, **92**, 1502–1510.
45 Y. Xiong, J. Huang, S.-T. Wang, S. Zafar and O. Gang, *ACS Nano*, 2020, **14**, 14646–14654.
46 B. J. Bennion and V. Daggett, *Proc. Natl. Acad. Sci. U. S. A.*, 2003, **100**, 5142.
47 F. S. Liao, W. S. Lo, Y. S. Hsu, C. C. Wu, S. C. Wang, F. K. Shieh, J. V. Morabito, L. Y. Chou, K. C. W. Wu and C. K. Tsung, *J. Am. Chem. Soc.*, 2017, **139**, 6530–6533.
48 D. E. Budil, S. Lee, S. Saxena and J. H. Freed, *J. Magn. Reson., Ser. A*, 1996, **120**, 155–189.
49 A. Ma, Z. Luo, C. Gu, B. Li and J. Liu, *Inorg. Chem. Commun.*, 2017, **77**, 68–71.
50 C. Tamames-Tabar, D. Cunha, E. Imbuluzqueta, F. Ragon, C. Serre, M. J. Blanco-Prieto and P. Horcajada, *J. Mater. Chem. B*, 2014, **2**, 262–271.
51 I. Abánades Lázaro, C. J. R. Wells and R. S. Forgan, *Angew. Chem., Int. Ed.*, 2020, **59**, 5211–5217.
52 E. S. Grape, J. G. Flores, T. Hidalgo, E. Martínez-Ahumada, A. Gutiérrez-Alejandre, A. Hautier, D. R. Williams, M. O'Keeffe, L. Öhrström, T. Willhammar, P. Horcajada, I. A. Ibarra and A. K. Inge, *J. Am. Chem. Soc.*, 2020, **142**, 16795–16804.
53 S. Wang, Y. Chen, S. Wang, P. Li, C. A. Mirkin and O. K. Farha, *J. Am. Chem. Soc.*, 2019, **141**, 2215–2219.